ARTHRITIS & RHEUMATISM
Vol. 65, No. 7, July 2013, pp 1786–1794
DOI 10.1002/art.37960

Long-Term Detection of Human Adipose-Derived Mesenchymal Stem Cells After Intraarticular Injection in SCID Mice

Karine Toupet,[1] Marie Maumus,[1] Julie-Anne Peyrafitte,[2] Philippe Bourin,[2] Peter L. E. M. van Lent,[3] Rosanna Ferreira,[4] Béatrice Orsetti,[5] Nelly Pirot,[6] Louis Casteilla,[7] Christian Jorgensen,[8] and Danièle Noël[1]

Objective. **Mesenchymal stem cells (MSCs) represent a promising tool for cell therapy for several disorders, among them the osteoarticular diseases. For such clinical applications, intraarticular (IA) injection of MSCs may be favored for higher levels of safety and targeting of specific joints. Although the safety of intravenous (IV) administration of MSCs has been reported in a number of clinical trials, the safety and biodistribution of MSCs after IA injection have not been tested. Our objective was to assess the toxicity of clinical-grade human adipose-derived MSCs (AD-MSCs), as well as their biodistribution, after IA injection into SCID mice.**

Methods. **SCID mice received IA or IV administration of 10^6 human AD-MSCs. Several tissues were recovered at different time points and processed for histologic assessment or real-time polymerase chain reaction (PCR) analysis. A highly sensitive assay was used to monitor the distribution of AD-MSCs, based on amplification of human-specific Alu sequences.**

Results. **Absence of toxicity was observed after AD-MSC infusion. Alu PCR assay revealed a high sensitivity (1 human AD-MSC/10^5 murine cells), with a large linear range (1–5 × 10^4/10^5 murine cells). Importantly, 15% of the IA-injected AD-MSCs were detectable in the joint for the first month and 1.5% of the AD-MSCs engrafted over the long term, at least 6 months. AD-MSCs were observed in the injected joints and in areas of tissue referred to as stem cell niches, such as the bone marrow, adipose tissue, and muscle.**

Conclusion. **These data support the feasibility and safety of using IA delivery of human AD-MSCs in the treatment of rheumatic diseases that affect the joints.**

During the last decade, multipotent mesenchymal stromal cells, also known as mesenchymal stem cells (MSCs), have attracted much attention for multiple applications in regenerative medicine. Such interest relies on their availability in diverse tissues, such as bone marrow (BM-MSCs) or adipose tissue (AD-MSCs), where they are found in high numbers and can be isolated using easy and reproducible procedures (1). They also garnered great interest because of their unique properties, in particular, their potential for differentiation toward cells belonging to the musculoskeletal lineages, allowing their use in tissue engineering. In addition, MSCs exhibit immunosuppressive properties and trophic functions that have prompted the develop-

Supported by the European Union Seventh Framework Programme (project Adipoa; FP7/2007-2013) and by the French National Research Agency (part of the Investments for the Future program; ANR-11-INBS-005). Work in the INSERM U844 laboratory was supported by the INSERM Institute, the University of Montpellier 1, and by project Adipoa (FP7/2007-2013).

[1]Karine Toupet, PhD, Marie Maumus, PhD, Danièle Noël, PhD: INSERM U844, Hôpital St. Eloi, and Université Montpellier 1, Montpellier, France; [2]Julie-Anne Peyrafitte, MSc, Philippe Bourin, MD, PhD (current address: CSA21, Toulouse, France): EFS Pyrénées-Méditerranée, Toulouse, France; [3]Peter L. E. M. van Lent, PhD: Radboud University Nijmegen Medical Centre, Nijmegen, The Netherlands; [4]Rosanna Ferreira, MD: Hôpital Lapeyronie, Montpellier, France; [5]Béatrice Orsetti, PhD: EMI 229 INSERM and Université Montpellier 1, Montpellier, France; [6]Nelly Pirot, PhD: IRCM, INSERM U896, Université Montpellier 1, and CRLC Val d'Aurelle–Paul Lamarque, Montpellier, France; [7]Louis Casteilla, PhD: EFS Pyrénées-Méditerranée, CNRS 5273, UMR STROMALab, Université Toulouse III Paul Sabatier, and INSERM U1031, Toulouse, France; [8]Christian Jorgensen, MD, PhD: INSERM U844, Hôpital St. Eloi, Université Montpellier 1, and Hôpital Lapeyronie, Montpellier, France.

Drs. Toupet and Maumus contributed equally to this work.

Address correspondence to Danièle Noël, PhD, INSERM U844, Hôpital St. Eloi, Bat INM, 80 Avenue Augustin Fliche, 34295 Montpellier Cedex 5, France. E-mail: daniele.noel@inserm.fr.

Submitted for publication June 22, 2012; accepted in revised form March 26, 2013.

ment of preclinical studies to test their efficacy in various inflammatory and degenerative diseases (2). Another interesting characteristic of these cells is their migration potential and capacity to be mobilized to sites of injury.

Both endogenous and exogenously delivered MSCs can migrate to areas of injury and participate in the repair process. The precise mechanisms underlying the migration of these cells into injured tissues are still not fully understood, although multiple signaling pathways and molecules have been reported (3). Exogenous mesenchymal progenitors may be injected via local or systemic routes. Systemic administration of BM-MSCs or AD-MSCs has been used in many experimental models and clinical trials because it allows minimally invasive delivery of the cells (4). However, exogenous MSCs localize differently depending on the model; they mainly home to the lung in naive animals, whereas they localize to the injured site in animal models of injuries (5,6).

After intravenous (IV) infusion, 83% of the infused cells are trapped in the lungs within 15 minutes and then rapidly disappear (half-life ~24 hours), mainly through apoptosis (4). Local delivery of MSCs may be of interest in situations in which they can be directly implanted in the injured site, where they can participate in tissue regeneration. Moreover, local administration theoretically offers other advantages over systemic administration: they should preferentially stay in the site of injection and, thus, be safer, and they should survive for a longer time. Little information on the survival and distribution of MSCs after local delivery is available, however, and no data are available on the long-term biodistribution of these cells after intraarticular (IA) injection.

IA injection of BM-MSCs or AD-MSCs is warranted for cell therapy strategies aiming at regenerating cartilage in patients with osteoarticular conditions. The therapeutic efficacy of AD-MSCs after IA delivery was recently demonstrated in murine models of posttraumatic arthritis or osteoarthritis (7,8). For clinical applications, the safety of the cell production process using good laboratory practice (GLP) conditions has to be guaranteed and is currently being validated (9). However, the fate of clinical-grade MSCs is still an open question and has been rarely evaluated in vivo.

In the present study, we evaluated the biodistribution and toxicity of human AD-MSCs produced under GLP conditions. We investigated the dynamics of AD-MSCs after IA versus IV administration in SCID mice and traced their homing to different organs, using quantitative and highly sensitive human Alu sequence–specific polymerase chain reaction (PCR) analysis. Using fluorescence in situ hybridization (FISH) assays, we definitively identified the presence of cells of human origin in the mouse joints. We then used a model of injury-mimicking chemotactism to assay the targeted mobilization of infused human AD-MSCs. Finally, we evaluated the toxicity of AD-MSC infusion via histopathologic analysis under GLP conditions.

MATERIALS AND METHODS

Isolation and characterization of AD-MSCs. Production of human AD-MSCs according to GLP conditions for therapeutic use was performed as recently described (9). All subjects who allowed the use of their tissue specimens for research purposes provided their informed consent before surgery. Briefly, adipose tissue obtained through liposuction was digested with collagenase at 37°C for 45 minutes. The stromal vascular fraction was then transferred into CellStack chambers at a density of 4,000 cells/cm^2 in α-minimum essential medium (α-MEM) supplemented with platelet lysate. On day 8, cells were trypsinized and expanded at 2,000 cells/cm^2 until day 14 (end of passage 1).

Cell counting and viability were performed on days 8 and 14 using trypan blue exclusion. Phenotyping was carried out by flow cytometry. Antibodies specific for CD markers were obtained from BD PharMingen (CD14, CD34, CD45, CD73, and CD90) or eBioscience (CD13, CD29, and CD105).

Differentiation of AD-MSCs. *Osteogenic differentiation.* Passage 1 AD-MSCs were plated at 2,000 cells/cm^2 and cultured for 3 weeks in α-MEM supplemented with 10% fetal calf serum (FCS), 0.1 μmole/liter of dexamethasone, 50 μmoles/liter of ascorbic acid, and 3 mmoles/liter of monobasic sodium phosphate. During the last week of culture, the monobasic sodium phosphate was replaced by β-glycerophosphate (10 mmoles/liter). Cultures were then rinsed with phosphate buffered saline (PBS), fixed with 10% formaldehyde, and matrix mineralization was visualized with alizarin red staining.

Adipogenic differentiation. Passage 1 AD-MSCs were plated at 2,000 cells/cm^2 until confluence. Culture medium was then replaced by α-MEM supplemented with 10% FCS, 1 μmole/liter of dexamethasone, 60 μmoles/liter of indomethacin, and 450 μmoles/liter of isobutylmethylxanthine (IBMX). After 3 days, the medium was replaced by induction medium without IBMX. After 20 days, cultures were rinsed with PBS, fixed with 10% formaldehyde, and lipid droplets were stained with oil red O.

Chondrogenic differentiation. Passage 1 AD-MSCs (250,000 cells) were cultured in pellet form in the presence of inductive medium, as described elsewhere (10,11). Differentiation was assessed by immunohistochemistry using antiaggrecan antibodies (1:50 dilution; Millipore) on paraffin sections of pellets.

Endothelial differentiation. Passage 1 AD-MSCs were plated at a density of 5,000 cells/ml in 1.5 ml of methylcellulose (MethoCult GF H4534; StemCell Technologies) for 20 days.

Injection of AD-MSCs into SCID mice. SCID/bg mice were housed and cared for according to the Laboratory Animal Care guidelines. Approval was obtained from the

Regional Ethics Committee on Animal Experimentation before initiation of the study (approval CEEA-LR-10042). Experiments were conducted in accordance with the Regional Ethics Committee on Animal Research and Care. For intraarticular injections, mice were anesthetized, and 10^6 AD-MSCs in 7 μl of PBS was delivered into both joint cavities using a 10-μl Hamilton syringe (NH-BIO). For intravenous infusions, 10^6, 2×10^6, or 4×10^6 AD-MSCs/100 μl of PBS was injected into the tail vein of groups of mice. Euthanasia was performed at different time points, and 14 organs (lung, heart, kidney, spleen, tibialis anterior muscle, brain, inguinal fat pad, BM, stomach, intestine, liver, testis or ovary, blood, knee joint) were harvested and rapidly frozen at –80°C. One knee joint was fixed in 4% formalin and processed for routine histology. When indicated, 1 μg of human stromal cell–derived factor 1 (SDF-1; R&D Systems) was injected into one tibialis anterior muscle on day 11 after administration of AD-MSCs, and the muscle and joint tissues were recovered after 2 days or 10 days for quantitative reverse transcription–PCR analysis.

DNA extraction and real-time PCR. Depending on their size, all or part of each organ was weighed, and a proportional amount of lysis buffer was added prior to mechanical dissociation using an Ultra-Turrax T-50 homogenizer. DNA extraction was performed on 180 μl of tissue suspension using a DNeasy Blood and Tissue kit (Qiagen) and quantified using a spectrophotometer (NanoDrop; Labtech). Real-time quantitative PCR (qPCR) was performed on 25 ng of DNA in a total volume of 10 μl containing 5 μl of DNA Master SYBR Green I kit (Roche Diagnostics) and 0.05 μM primers for Alu or 0.5 μM for murine actin. The primer sequences used were as follows: for human Alu, 5′-CATGGTGAAACCCCGTCTCTA-3′ (forward) and 5′-GCCTCAGCCTCCCGAGTAG-3′ (reverse) (4,12) and for murine actin, 5′-GATGCACAGTAGGTCTAAGTGGAG-3′ (forward) and 5′-CACTCAGGGCAGGTGAAACT-3′ (reverse). PCR conditions were as follows: 95°C for 15 minutes, followed by 40 cycles at 95°C for 15 seconds and 64°C for 30 seconds and then 40°C for 30 seconds. Standard curves were generated by adding 10-fold serial dilutions of human AD-MSCs in murine MSCs (the total cell number was kept constant at 10^6 cells) to determine the number of human AD-MSCs in the 25 ng of DNA that was used in the PCR reaction for each organ. According to the quantity of DNA isolated from the organ, we extrapolated the number of human AD-MSCs per organ, and this value was then normalized to the average weight of each organ. The results were then expressed as the percentage of human AD-MSCs per organ, per 1.5 ml of circulating blood, or per total bone marrow (flushed from 1 femur).

Histologic assessment. After euthanasia, the hind limbs were collected, fixed in 4% formaldehyde, and processed for routine histologic assessment. Paraffin sections were stained with hematoxylin and eosin.

Hybridization with labeled Cot-1 DNA. Tissue sections were placed in citrate buffer, pH 6, at 100°C for 20 minutes and then treated with pepsin for 15 minutes (Kreatech). Sections were hybridized with human (Roche) and mouse (Life Technologies) Cot-1 DNA that had been labeled using a FISHBright 550 Red/Orange and a FISHBright 495 Green labeling kit, respectively (Kreatech). Aliquots containing 100 ng of each probe were coprecipitated with herring sperm DNA and resuspended in 10 μl of paraffin hybridization buffer (Kreatech). The probe was codenatured with the tissue sections at 80°C for 5 minutes and hybridized in a humidified chamber at 37°C for 16 hours. Slides were washed, stained with DAPI, and after a FISH digestion protocol (Kreatech), mounted.

Toxicology study. One group of 10 male and 10 female SCID mice was given a single IV injection of human AD-MSCs (2×10^6 cells/100 μl of PBS), and these mice were compared with 10 male and 10 female control SCID mice. Five mice of each sex were killed on day 14, and the remaining mice were killed on day 90. The following organs and tissues were harvested and fixed in 4% formalin: tail (injection site), hind limb, skin/subcutis, liver, gall bladder, kidney, heart, lung, spleen, thymus, popliteal lymph node, ovary, uterus, vagina, testis, prostate, skeletal muscle, pancreas, esophagus, glandular and nonglandular stomach, duodenum, jejunum, ileum, cecum, colon, rectum, thyroid, trachea, and brain. Organs were trimmed according to the procedures recommended by the Registry of Industrial Toxicology Animal-data (RITA) and the North American Control Animal Database (NACAD). Sections (4 μm) were stained with hematoxylin and eosin. All analyses were GLP compliant and were performed in the Clinical Pathology Laboratory of Sanofi-Aventis Research and Development (Montpellier, France).

Analysis of biochemical parameters. For biochemical parameter evaluation, blood samples from mice euthanized on day 90 were collected into tubes containing lithium/heparin, and plasma samples were prepared. The clinical chemistry parameters were evaluated using a Cobas 6000 c501 automated analyzer (Roche Diagnostics). The following clinical chemistry parameters were examined: aspartate aminotransferase (AST), alanine aminotransferase (ALT), alkaline phosphatase, total bilirubin, total cholesterol, triglycerides, glucose, urea, creatinine, total protein, and albumin. All measures and analyses were GLP compliant and performed in the Clinical Pathology Laboratory of Sanofi-Aventis Research and Development.

Statistical analysis. Statistical analysis was performed with GraphPad Software. Values are reported as the mean ± SEM of separate experiments. Comparison between several groups was performed by one-way analysis of variance, followed by Dunnett's post hoc test or Student's *t*-test for 2 groups. *P* values less than 0.05 were considered significant.

RESULTS

Phenotype of culture-expanded human AD-MSCs. Human AD-MSCs were isolated from abdominal subcutaneous fat tissue, expanded in platelet lysate under GLP conditions (9). Under these culture conditions, AD-MSCs reached subconfluence on day 8 (end of passage 0), with a mean ± SEM population-doubling time of 29.1 ± 4 (n = 3 samples). Following trypsin digestion and replating, cells reached the end of passage 1 after 6 days, with a population-doubling time of 38.1 ± 2.8 (n = 3 samples). The mean ± SEM cell viability was 99.7 ± 0.4% at passage 0 and 98.8 ± 1.0% at passage 1.

At the end of passage 1, phenotype characterization of the human AD-MSCs demonstrated a homoge-

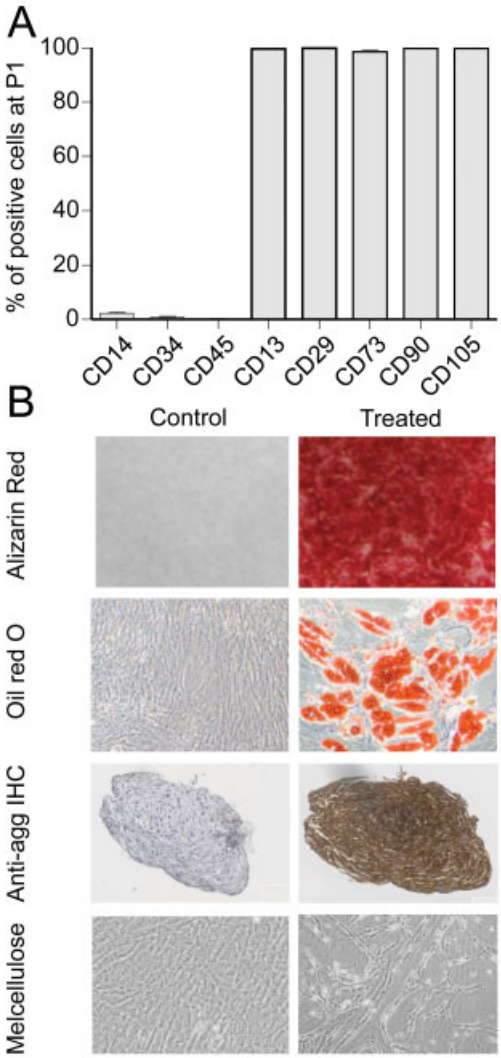

Figure 1. Characterization of human adipose-derived mesenchymal stem cells (AD-MSCs) at passage 1. **A,** Immunophenotype of the AD-MSCs, as assessed by flow cytometry. Values are the mean ± SEM of 3 samples. **B,** Differentiation potential of AD-MSCs, as visualized with alizarin red staining, indicating osteogenic lineage, oil red O staining, indicating adipogenic lineage, antiaggrecan (anti-agg) immunohistochemistry (IHC), indicating chondrogenic lineage, and culture in semisolid methylcellulose (melcellulose) medium, indicating endothelial-like morphology. Original magnification × 50. Color figure can be viewed in the online issue, which is available at http://onlinelibrary.wiley.com/doi/10.1002/art.37960/abstract.

neous population of cells negative for CD14, CD34, and CD45 and positive for CD13, CD29, CD73, CD90, and CD105 (Figure 1A). The differentiation potential of passage 1 human AD-MSCs toward the osteogenic, adipogenic, chondrogenic, and endothelial lineages was tested under specific inductive conditions. Osteogenic, adipogenic, and chondrogenic differentiations were demonstrated, respectively, by alizarin red staining for matrix mineralization, oil red O staining for lipid accumulation, and antiaggrecan immunohistochemical staining for specific cartilage matrix (Figure 1B). Culture of human AD-MSCs in semisolid methylcellulose medium demonstrated an endothelial-like differentiation (Figure 1B).

Sensitivity and reproducibility of Alu real-time PCR. To quantify human AD-MSCs, we relied on the use of real-time PCR for human-specific Alu sequences, as described previously (4,12). Quantitative PCR was performed with 25 ng of DNA isolated from serial 10-fold dilutions of human AD-MSCs in murine MSCs ranging from 0.0005% to 50% human AD-MSCs in the mixture. Specificity of Alu primers was verified by the absence of PCR product when running the PCR with murine DNA as template (data not shown). The relationship between the number of human AD-MSCs and the Alu signal was excellent, with a correlation coefficient of r = –0.9996 between 0.005% and 50% human AD-MSCs (Figure 2A). The detection limit was 0.005% of human AD-MSCs in the total cell mixture, which corresponds to 0.1 human AD-MSC in 25 ng of DNA.

We then evaluated whether different preparations of human AD-MSCs contained comparable amounts of Alu copies. Quantitative PCR was performed with DNA from 4 samples of human AD-MSCs that had been serially diluted in murine MSCs as above. Comparable amounts of Alu-specific sequences were amplified in the different cell preparations according to the percentage of human AD-MSCs in the mixture (Figure 2B). The correlation coefficient was r = –0.991, and the detection limit was again 0.005% of human AD-MSCs in the mixture. These results strongly support the idea that this technique can be used to quantify human AD-MSCs after administration in mice.

Biodistribution of human AD-MSCs after IA administration in SCID mice. Evaluation of the biodistribution of human AD-MSCs after intraarticular administration into SCID mice was performed on days 11, 28, 90, and 186. Cell engraftment was quantified in 14 organs through the detection of human-specific Alu sequences and normalization using murine actin sequences. First, the distribution of human AD-MSCs in the various organs was expressed as the percentage of mice that retained human AD-MSCs in a specific organ at each time point tested (Figure 3A). Human AD-MSCs were detected in the joint in 90–100% of mice for the first 3 months and were still observed in 60% of the mice after 6 months. Human cells were never detected in the lung, kidney, stomach, or liver. They were observed in the heart, spleen, intestine, brain, blood, or testis in

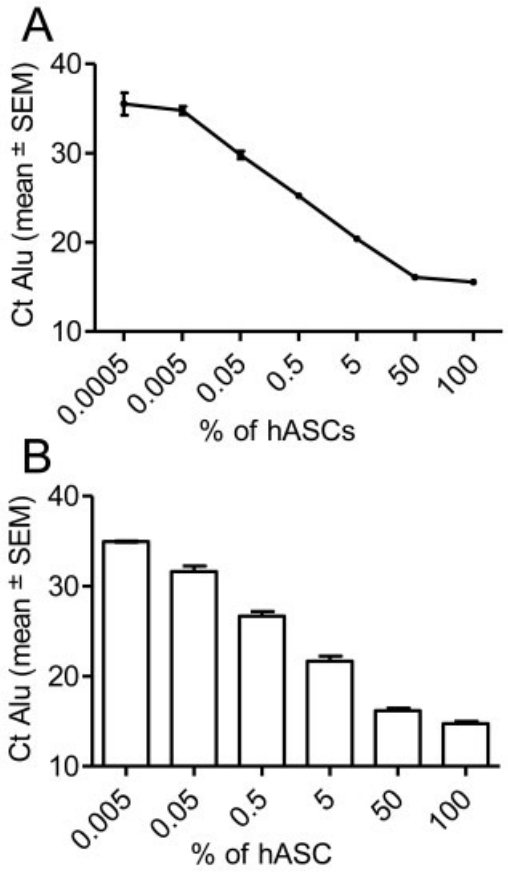

Figure 2. Quantification of human adipose-derived mesenchymal stem cells (AD-MSCs [hASCs]) according to Alu sequence determination. **A,** Determination of the number of Alu sequences according to the percentage of human AD-MSCs in mixed populations of human AD-MSCs and murine MSCs (n = 16 replicates). **B,** Quantification of Alu sequences in separate biologic samples (n = 4 individuals).

10–20% of mice, but only at 1 or 2 time points. In contrast, the cells engrafted in the muscle, fat, and bone marrow in 10–30% of mice for the first 3 months and were still present in the muscle and adipose tissue at 6 months.

Next, the distribution of human AD-MSCs at each time point was expressed as the percentage of cells detected in the organs as compared with the initial number of injected cells (Figure 3B). Importantly, 15% of the injected human AD-MSCs were found in various organs on day 11 and day 28, whereas 1.5% were still observed after 6 months. As expected, the highest numbers of human cells were recovered at the site of injection; ~13% of the injected human AD-MSCs stayed in the joints during the first month, and 1.3% were still detected at months 3 and 6. The presence of human cells was found predominantly and consistently in the bone marrow, adipose tissue, and muscle. In some rare cases, human AD-MSCs were found at a rather high level in the intestine, brain, or spleen (in only 1 mouse; 10 mice injected).

To confirm that the quantities of the Alu sequences could be attributed to the presence of human AD-MSCs and not DNA fragments that could be internalized by endogenous cells, we performed histologic analyses. In the intraarticular space of the joint, high numbers of cells were detected that were mainly localized in the synovial recesses, on the edges of the articular cartilage, or at the surface of the articular cartilage at all time points tested (Figures 4A–D). FISH analysis was used to verify the human origin of the cells detected in the intraarticular space. We observed high numbers of cells positive for human nuclei, as shown by a red fluorescent signal, as compared with the corresponding

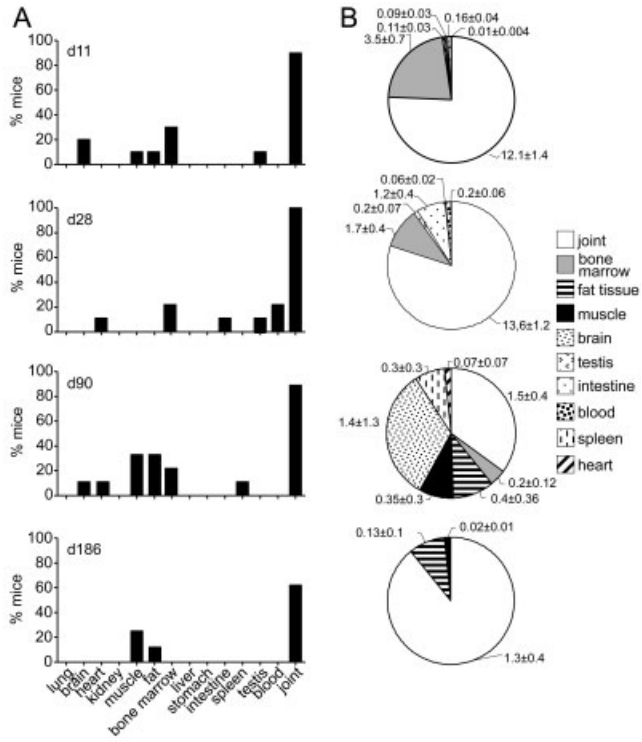

Figure 3. Biodistribution of human adipose-derived mesenchymal stem cells (AD-MSCs) on days 11, 28, 90, and 186 after intraarticular injection into SCID mice. **A,** Percentages of mice in which human AD-MSCs were detected in the indicated organs at the time points tested. **B,** Percentages of human AD-MSCs present in the indicated organs, as determined by Alu sequence quantification. Values are the mean ± SEM percentage of human AD-MSCs retained of the total number injected.

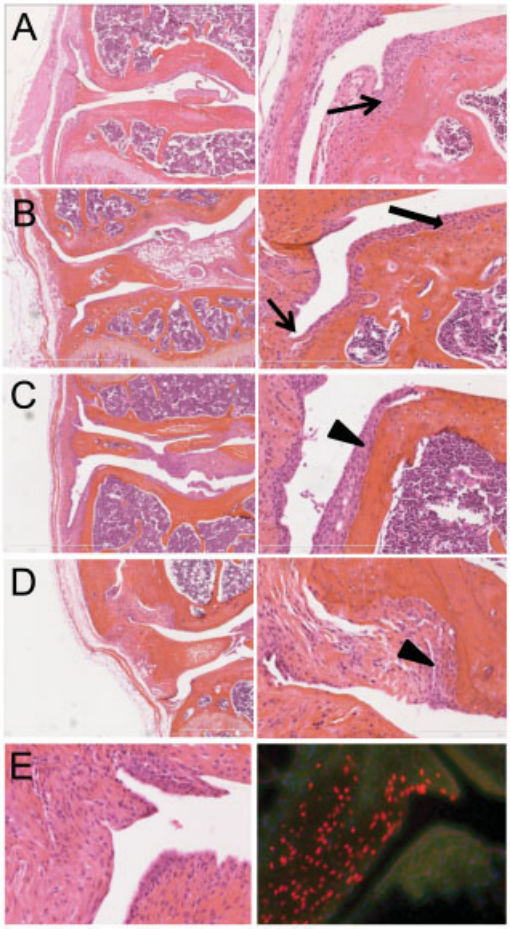

Figure 4. Histologic analysis of joints from SCID mice treated with human adipose-derived mesenchymal stem cells. **A–D,** Injected cells observed in the synovial recesses (**arrows**) and at the surface (**thick arrow**) or edges (**arrowheads**) of the articular cartilage on day 11 (**A**), day 28 (**B**), day 90 (**C**), and day 186 (**D**). Hematoxylin and eosin (H&E) stained; original magnification × 5 (left) or × 20 (right). **E,** H&E staining (left) and fluorescence in situ hybridization (right) of human (red) and murine (green) cells in joint sections obtained on day 28. Original magnification × 20.

murine cells, as shown by a green fluorescent signal (Figure 4E).

Finally, to evaluate whether human AD-MSCs were functional after IA engraftment, we investigated the possibility of attracting them to a predetermined site. Injection of human SDF-1 was used to mimic the release of chemokines that occurs following injury, and we evaluated the number of emigrating human AD-MSCs. Thus, human SDF-1 was injected into the tibialis anterior muscle and PBS was injected into the contralateral tibialis anterior muscle of mice that had received IA injections of human AD-MSCs 11 days previously. The Alu sequences were quantified 3–10 days later. Human AD-MSCs were detected in the joints of all 8 mice in this experimental group, as well as in 3 of the 8 PBS-injected muscles and 5 of the 8 human SDF-1–injected muscles in this experimental group. Importantly, 63% of mice had an AD-MSC ratio of >1 for the SDF-1–injected versus the PBS-injected muscle, whereas 25% of mice had a ratio of <1. These data indicate a high level of AD-MSC migration toward the human SDF-1–injected muscle, indicating that the cells were able to actively emigrate from their niches. In summary, after IA injection of human AD-MSCs, we found that the cells engrafted over the long term in the injected joints and tissues known to be stem cell niches (i.e., the bone marrow, adipose tissue, and muscle) and were functional at least over the short term.

Biodistribution of human AD-MSCs after IV infusion in SCID mice. In order to compare the biodistribution of human AD-MSCs after local or systemic administration, we injected different amounts of cells (10^6, 2×10^6, or 4×10^6) into the tail vein of SCID mice. An absence of toxicity was recorded at the lowest two doses, but when 4×10^6 AD-MSCs were infused, 2 of the 9 mice in the experimental group died of embolism at the time of injection. We then quantified the number of human AD-MSCs in the different organs on day 11 and day 28 following IV infusion. The number of injected human AD-MSCs (10^6, 2×10^6, or 4×10^6) had no influence on the tissue localization or the number of mice in which cells could be detected. Data from the 3 groups of mice were therefore pooled.

The most striking observation was the rapid clearance of the human AD-MSCs after IV injection, since no human cells could be detected in 7 of the 12 mice on day 11 and in 8 of 12 mice on day 28. While human AD-MSCs were not detected in the kidney, muscle, fat, testis, or blood, they were found in the heart, spleen, brain, bone marrow, intestine, or liver at 1 of the 2 time points in 8% of the mice (Figure 5A). The cells were always detected in the lung (17% of mice on day 11 and 25% on day 28) and were detected in the joint in 17% of the mice on day 11. Apart from the lung (0.03% and 0.3% of the injected AD-MSCs on day 11 and day 28, respectively), the highest percentage of human cells was found in the intestine (1.1% on day 11), liver (0.15% on day 11), and stomach (0.4% on day 28) (Figure 5B). Indeed, after IV administration, 98.5% of the human AD-MSCs disappeared before day 11, and the remaining cells were mostly observed in the lung and the gastrointestinal tract.

Safety and toxicity of IV administration. We next evaluated the safety and toxicity of administration of human AD-MSCs according to biochemical parameters in the blood plasma of the treated mice as well as an extensive histopathologic examination at necropsy. We chose IV injection to evaluate the safety under the worst conditions, where human AD-MSCs may migrate systemically. The weight of the mice was measured at 1-week intervals during experimentation, and the weights were similar in the control and AD-MSC–treated groups. Mice were euthanized on day 14 (short term) or day 90 (midterm) after IV injection of human AD-MSCs. On day 90, we evaluated 11 biochemical parameters in the plasma of mice to detect any possible toxic effect over the long term. Most of the parameters we tested showed no statistically significant differences in female versus male mice or in AD-MSC–treated versus control groups. However, we observed a significant decrease in glucose levels in the AD-MSC–treated group, but only in the male mice, whereas the triglyceride levels were significantly reduced in the female mice receiving human AD-MSCs (Figures 6A–C). Although significantly higher levels of AST were detected in male mice treated with AD-MSC, the ratios of AST to ALT were not statistically different in AD-MSCs–treated versus control groups whatever the sex, reflecting the absence of hepatotoxicity induced by administration of human AD-MSCs.

At necropsy performed on the short-term and midterm groups, histopathologic examination of the selected organs did not reveal any findings related to the human AD-MSCs. However, some findings were attributed to the immunodeficiency and spontaneous pathology of the SCID mice (lymphoblastic thymoma [13]; mild or moderate osteoarthritis of the knee joint in 1 mouse in both groups [14]). Of importance, an absence of induced preneoplastic or neoplastic lesions was recorded at the end of experimentation. Taken together, the findings of the histopathologic analysis support the absence of any human AD-MSCs–related lesions or neoplasia on day 14 and on day 90 after IV administration of human AD-MSCs.

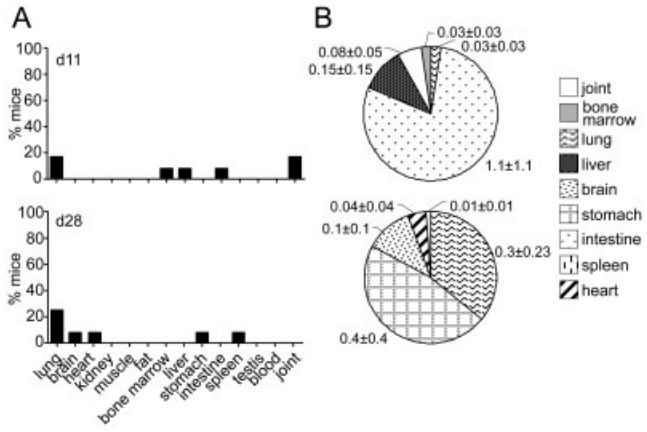

Figure 5. Biodistribution of human adipose-derived mesenchymal stem cells (AD-MSCs) on days 11 and 28 after intravenous injection into SCID mice. **A,** Percentages of mice in which human AD-MSCs were detected in the indicated organs at the time points tested. **B,** Percentages of human AD-MSCs present in the indicated organs, as determined by Alu sequence quantification. Values are the mean ± SEM percentage of human AD-MSCs retained of the total number injected.

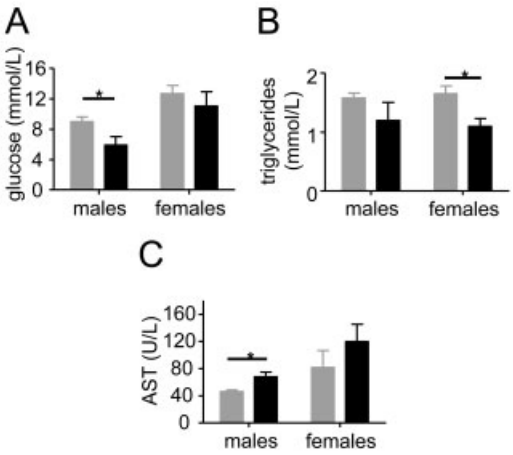

Figure 6. Biodistribution of human adipose-derived mesenchymal stem cells after intravenous injection (solid bars) in SCID mice as compared with control, uninjected mice (shaded bars), by sex. Plasma levels of **A,** glucose, **B,** triglycerides, and **C,** aspartate aminotransferase (AST) were determined in samples obtained on day 90. Values are the mean ± SEM of 5 mice per group. $* = P < 0.05$.

DISCUSSION

This study is the first to examine the safety and long-term persistence of clinical-grade human AD-MSCs after IA administration. Importantly, most of the exogenous human AD-MSCs remained at the site of injection, with a number of cells migrating preferentially to the stem cell niches, including bone marrow, adipose tissue, and muscle.

We used a simple, accurate, and sensitive method to track unmodified human AD-MSCs: human Alu-specific sequence detection and real-time PCR (4,12). This allowed us to avoid possible artifacts due to the use of cells that are genetically engineered to express reporter transgenes and may therefore be functionally altered. Although PCR analyses were easier to initiate, cell tracking using magnetic resonance imaging would

have been of interest for the detection of single cells in vivo, but it would require prior labeling of the cells with iron oxide particles, and such labeling has been found to interfere with the actin cytoskeleton, resulting in reduced viability and migration potential of MSCs (15). Moreover, in a model of experimental autoimmune encephalomyelitis, treatment using iron oxide–labeled MSCs led to an increase in disease severity due to surface-bound iron detachment from the MSCs (16). Under the conditions used in our study, Alu-specific PCR allowed the detection of as few as 1 human AD-MSC out of 100,000 murine cells and with high reproducibility.

While the safety of IV injection of MSCs has been confirmed in a large number of patients enrolled in several clinical studies for conditions such as graft-versus-host disease (17), heart disease (18), or autoimmune disease (19), the fate of stem cells after infusion still remains unclear. To address this issue, a number of studies have been initiated in different preclinical models. A previous study reported that 99% of IV-infused MSCs were cleared from the circulation within 5 minutes, and after 15 minutes, 83% of human MSCs were recovered in lungs, with only trace amounts in other tissues (4). Most of the models, including the aforementioned one, relied on the use of immunodeficient mice, with or without sublethal irradiation (20), mice subjected to immunosuppressant conditioning (21), or neonatal mice (22).

In the present study, we used immunodeficient SCID mice so as to more closely mimic conditions of autologous human AD-MSC transplantation in the clinic, where no immune rejection is expected. The most important finding was that most of the human AD-MSCs (99%) were eliminated during the first 10 days. The greatest numbers of human AD-MSCs were seen in the lung, gastrointestinal tract (intestine, stomach, liver), brain, and heart. This is consistent with observations reported by others in short-term studies, where high and transient retention of MSCs in the lungs occurred during the first 24–48 hours, followed by redistribution to the liver, spleen, brain, or heart (20,23,24). Infused MSCs mainly localized in the lungs because of the cell size and receptor-mediated adhesion (23,24). Importantly, we show here that infusion of human AD-MSCs is safe, since no hepatic or renal toxicity was apparent, and no histopathologic or neoplastic findings were recorded after 3 months.

In contrast to IV infusion of the cells, IA injection allowed the persistence of 15% of the human AD-MSCs for the first month, with 1.5% remaining after 6 months. The biodistribution of the cells was different between the two routes of administration, with maximal levels of joint engraftment in all mice during the first 3 months. Persistence of human AD-MSCs in the joints of 60% of the animals was still observed after 6 months, demonstrating a high rate of cell survival in the joint space environment. Using both immunohistochemistry and FISH, we localized the AD-MSCs inside the synovial membrane, demonstrating engraftment within the tissue over the long term. Although not previously reported, AD-MSC engraftment in the joint is not surprising, since synovium is known to be a niche for MSCs (25,26). It has been proposed that following injury, MSCs migrate from the synovial membrane toward the damaged cartilage, differentiate into chondrocytes, and participate in tissue regeneration (27). Indeed, the joint supplies an appropriate environment that allows the survival of human AD-MSCs over the long term.

In the present study, a proportion of human AD-MSCs delivered IA migrated and homed within the BM. Compared with IV injection, where the human AD-MSCs were recovered in 10% of the mice on day 11, with IA administration, human AD-MSCs were still detected in 20–30% of the mice after 3 months. Although some studies have shown the presence of MSCs in the BM after infusion (23,28–30), BM homing of AD-MSCs was not commonly described, even following sublethal irradiation (20,22). Only 1 study mentioned BM as a highly targeted organ by exogenously infused AD-MSCs in mice that had undergone strong immunosuppressant conditioning (21).

Aside from migration through vascularized synovium, human AD-MSCs may also traffic toward the BM through canals that exist within the bone. Indeed, it has been reported that in the collagen-induced arthritis model before the onset of the disease, progenitor mesenchymal cells reside in the BM adjacent to the joint, in the synovium itself, and within enlarged bone canals that connect the BM to the synovium (31). This supports a direct connection between the two stem cell niches and suggests that human AD-MSCs might migrate to the BM through the preexisting canals. These observations also support the feasibility and safety of using human AD-MSCs for the treatment of rheumatic diseases that affect the joints.

ACKNOWLEDGMENTS

We thank Emmanuelle Arnaud for her help with the real-time PCR analyses and we thank the Réseau des Animaleries de Montpellier animal facility and the Réseau

d'Histologie Expérimentale de Montpellier histology facility, in particular, Yohan Noël, for processing the animal tissues.

AUTHOR CONTRIBUTIONS

All authors were involved in drafting the article or revising it critically for important intellectual content, and all authors approved the final version to be published. Dr. Toupet had full access to all of the data in the study and takes responsibility for the integrity of the data and the accuracy of the data analysis.

Study conception and design. Jorgensen, Noël.

Acquisition of data. Toupet, Maumus, Peyrafitte, Ferreira, Orsetti, Pirot.

Analysis and interpretation of data. Bourin, van Lent, Casteilla, Jorgensen, Noël.

REFERENCES

1. Tarte K, Gaillard J, Lataillade JJ, Fouillard L, Becker M, Mossafa H, et al. Clinical-grade production of human mesenchymal stromal cells: occurrence of aneuploidy without transformation. Blood 2010;115:1549–53.
2. Maumus M, Guerit D, Toupet K, Jorgensen C, Noel D. Mesenchymal stem cell-based therapies in regenerative medicine: applications in rheumatology. Stem Cell Res Ther 2011;2:14.
3. Li L, Jiang J. Regulatory factors of mesenchymal stem cell migration into injured tissues and their signal transduction mechanisms. Front Med 2011;5:33–9.
4. Lee RH, Pulin AA, Seo MJ, Kota DJ, Ylostalo J, Larson BL, et al. Intravenous hMSCs improve myocardial infarction in mice because cells embolized in lung are activated to secrete the anti-inflammatory protein TSG-6. Cell Stem Cell 2009;5:54–63.
5. Saito T, Kuang JQ, Bittira B, Al-Khaldi A, Chiu RC. Xenotransplant cardiac chimera: immune tolerance of adult stem cells. Ann Thorac Surg 2002;74:19–24.
6. Mouiseddine M, Francois S, Semont A, Sache A, Allenet B, Mathieu N, et al. Human mesenchymal stem cells home specifically to radiation-injured tissues in a non-obese diabetes/severe combined immunodeficiency mouse model. Br J Radiol 2007;80: S49–55.
7. Diekman BO, Wu CL, Louer CR, Furman BD, Huebner JL, Kraus VB, et al. Intra-articular delivery of purified mesenchymal stem cells from C57BL/6 or MRL/MpJ superhealer mice prevents post-traumatic arthritis. Cell Transplant 2012. E-pub ahead of print.
8. Ter Huurne M, Schelbergen R, Blattes R, Blom A, de Munter W, Grevers LC, et al. Antiinflammatory and chondroprotective effects of intraarticular injection of adipose-derived stem cells in experimental osteoarthritis. Arthritis Rheum 2012;64:3604–13.
9. Bourin P, Peyrafitte JA, Fleury-Cappellesso S. A first approach for the production of human adipose tissue-derived stromal cells for therapeutic use. Methods Mol Biol 2011;702:331–43.
10. Estes BT, Diekman BO, Gimble JM, Guilak F. Isolation of adipose-derived stem cells and their induction to a chondrogenic phenotype. Nat Protoc 2010;5:1294–311.
11. Djouad F, Delorme B, Maurice M, Bony C, Apparailly F, Louis-Plence P, et al. Microenvironmental changes during differentiation of mesenchymal stem cells towards chondrocytes. Arthritis Res Ther 2007;9:R33.
12. McBride C, Gaupp D, Phinney DG. Quantifying levels of transplanted murine and human mesenchymal stem cells in vivo by real-time PCR. Cytotherapy 2003;5:7–18.
13. Monticello TM, Green DS, Yang H, Drain RL, Franco CT, Durham SK. Spontaneous thymic lymphoma in severe combined immunodeficiency (SCID) mice engrafted with human peripheral blood lymphocytes. Vet Pathol 1994;31:393–5.
14. Walton M. Degenerative joint disease in the mouse knee; histological observations. J Pathol 1977;123:109–22.
15. Nohroudi K, Arnhold S, Berhorn T, Addicks K, Hoehn M, Himmelreich U. In vivo MRI stem cell tracking requires balancing of detection limit and cell viability. Cell Transplant 2010;19: 431–41.
16. Schafer R, Ayturan M, Bantleon R, Kehlbach R, Siegel G, Pintaske J, et al. The use of clinically approved small particles of iron oxide (SPIO) for labeling of mesenchymal stem cells aggravates clinical symptoms in experimental autoimmune encephalomyelitis and influences their in vivo distribution. Cell Transplant 2008;17:923–41.
17. Kebriaei P, Robinson S. Treatment of graft-versus-host-disease with mesenchymal stromal cells. Cytotherapy 2011;13:262–8.
18. Choi YH, Kurtz A, Stamm C. Mesenchymal stem cells for cardiac cell therapy. Hum Gene Ther 2011;22:3–17.
19. Sun L, Wang D, Liang J, Zhang H, Feng X, Wang H, et al. Umbilical cord mesenchymal stem cell transplantation in severe and refractory systemic lupus erythematosus. Arthritis Rheum 2010;62:2467–75.
20. Meyerrose TE, De Ugarte DA, Hofling AA, Herrbrich PE, Cordonnier TD, Shultz LD, et al. In vivo distribution of human adipose-derived mesenchymal stem cells in novel xenotransplantation models. Stem Cells 2007;25:220–7.
21. Kim DH, Je CM, Sin JY, Jung JS. Effect of partial hepatectomy on in vivo engraftment after intravenous administration of human adipose tissue stromal cells in mouse. Microsurgery 2003;23: 424–31.
22. Liao X, Li F, Wang X, Yanoso J, Niyibizi C. Distribution of murine adipose-derived mesenchymal stem cells in vivo following transplantation in developing mice. Stem Cells Dev 2008;17: 303–14.
23. Gao J, Dennis JE, Muzic RF, Lundberg M, Caplan AI. The dynamic in vivo distribution of bone marrow-derived mesenchymal stem cells after infusion. Cells Tissues Organs 2001;169:12–20.
24. Fischer UM, Harting MT, Jimenez F, Monzon-Posadas WO, Xue H, Savitz SI, et al. Pulmonary passage is a major obstacle for intravenous stem cell delivery: the pulmonary first-pass effect. Stem Cells Dev 2009;18:683–92.
25. Karystinou A, Dell'Accio F, Kurth TB, Wackerhage H, Khan IM, Archer CW, et al. Distinct mesenchymal progenitor cell subsets in the adult human synovium. Rheumatology (Oxford) 2009;48: 1057–64.
26. Djouad F, Bony C, Haupl T, Uze G, Lahlou N, Louis-Plence P, et al. Transcriptional profiles discriminate bone marrow-derived and synovium-derived mesenchymal stem cells. Arthritis Res Ther 2005;7:R1304–15.
27. Kurth TB, Dell'Accio F, Crouch V, Augello A, Sharpe PT, De Bari C. Functional mesenchymal stem cell niches in adult mouse knee joint synovium in vivo. Arthritis Rheum 2011;63:1289–300.
28. Bensidhoum M, Chapel A, Francois S, Demarquay C, Mazurier C, Fouillard L, et al. Homing of in vitro expanded Stro-1^- or Stro-1^+ human mesenchymal stem cells into the NOD/SCID mouse and their role in supporting human CD34 cell engraftment. Blood 2004;103:3313–9.
29. Allers C, Sierralta WD, Neubauer S, Rivera F, Minguell JJ, Conget PA. Dynamic of distribution of human bone marrow-derived mesenchymal stem cells after transplantation into adult unconditioned mice. Transplantation 2004;78:503–8.
30. Feng SW, Lu XL, Liu ZS, Zhang YN, Liu TY, Li JL, et al. Dynamic distribution of bone marrow-derived mesenchymal stromal cells and change of pathology after infusing into mdx mice. Cytotherapy 2008;10:254–64.
31. Marinova-Mutafchieva L, Williams RO, Funa K, Maini RN, Zvaifler NJ. Inflammation is preceded by tumor necrosis factor–dependent infiltration of mesenchymal cells in experimental arthritis. Arthritis Rheum 2002;46:507–13.